Carbon nanoparticles for study complex optical fields

O. V. ANGELSKY[a,b], C. Yu. ZENKOVA[a,b,*], D. I. IVANSKY[b], V. M. TKACHUK[b], JUN ZHENG[a]
[a]*Research Institute of Zhejiang University-Taizhou, China*
[b]*Chernivtsi National University, Chernivtsi, Ukraine*

In this research we propose a new approach to solve the problem of diagnosing complex optical fields by using carbon nanoparticles obtained experimentally by the bottom-up method. These nanoparticles have a size of about λ/10 and are characterized by a number of interesting optical properties: strong absorption and luminescence in the yellow-green region of the spectrum and weak absorption at the He-Ne laser radiation wavelength. These particular features made it possible to use these nanoparticles to determine the localization (diagnostics) of the points of phase singularities of the studied optical field and to reconstruct the distribution of the field intensity. The results of both a model experiment and computer simulation, which enabled to demonstrate the effectiveness of the proposed approach are proposed in the given paper. As a result of computer simulation, an inhomogeneous surface with the corresponding optical field in the form of a spatial distribution were synthesized. The use of Hilbert transform allowed reconstructing the phase map of the optical field with high accuracy.

(Received December 2, 2020; accepted June 11, 2021)

Keywords: Speckle-field, Optical singularity, Carbon nanoparticle, Hilbert transform

1. Introduction

The last decades have been marked by a surge of scientific activity in the development and study of carbon materials. This is reflected in their targeted synthesis, guided by the approach of forming a clearly defined nanostructure, which finds its application in the creation of multifunctional materials with unique optical, electronic, spin and photoelectric properties due to quantum size and edge effects. The possibility of using these structures in bioimaging, cancer therapy, temperature measurement, drugs delivery, biosensors production, as well as in photodetectors, solar cells, and photoluminescent materials is expanding.

Carbon nanoparticles (CNPs), selected from the existing list of carbon materials, as a separate form, which is characterized by a highly ordered structure [1], make up the object of research in this work. Unlike fullerenes, nanodiamonds, and carbon nanotubes, carbon nanoparticles are structures with defects and inhomogeneities, which, in fact, determine the properties of these nanoparticles [1]. These nanoobjects are assumed to have no definite shape, but they rather represent nanofragments of graphene that, in addition to hexagonal fragments, contain defect regions affecting the luminescent properties of particles [1]. It is due to the lack of a definite shape that carbon nanoparticles have a developed defect surface. This gives rise to interesting luminescent properties, opening up broad prospects for potential applications. In particular, their use in the biomedical field for visualization of cells and tissues or in industrial applications, as well as in the study of optical fields for diagnosing objects in aerodynamic and space research, is widely considered.

Optical trapping, as a new tool for manipulating and moving nanostructures, has been successfully applied to carbon nanoobjects [2, 3]. The variety of mechanisms of spatial displacement of such nanostructures is determined by the interaction of the laser field with instantly induced dipole momentum of individual molecules of the carbon nanosystems. Development in this direction served as an impetus for demonstrating the latest results of our research, the possibilities of diagnosing the structure of complex optical fields formed as a result of scattering of coherent radiation by surfaces with roughness. It also enabled to diagnose and to restore the intensity and phase distribution of the field in real time.

2. Statement of the problem

The interest in CNPs and the possibility of their use in our studies is determined by a set of factors, such as a small size of particles, the absence of expensive stages of their synthesis, the availability of a wide range of starting materials for their preparation, and the absence of toxic components in the process of synthesis. Structural analysis shows that all carbon nanoparticles have similarities in their structure. However, different methods of synthesis [3-6] lead to a significant variety of the degree of ordering of graphene fragments in CNPs, which causes the formation of the particles with complex morphology.

According to [7], we can talk about the following classification of CNPs: carbon nanoparticles, nanosized particles that do not exhibit quantum-dimensional properties; carbon quantum dots, nanoparticles with quantum-dimensional properties and crystalline structure; graphene quantum dots with pronounced edge effects.

The most interesting property of CNPs is their luminescence, which stimulates the following approach in the classification of carbon nanoparticles.

According to the existing classification [8], fluorescent nanoparticles can be divided into four types, such as

semiconductor quantum dots (SQDs), graphene quantum dots (GQDs), carbon quantum dots (CQDs) and carbon nanodots (CNDs).

Carbon-based quantum dots consisting of graphene quantum dots (QGDs) and carbon quantum dots (CQDs, C-dots or CDs) are a new class of carbon nanomaterials with sizes below 10 nm.

As a rule, the term *carbon dots* are used to denote a rather diverse class of materials, the structure and properties of which can vary greatly for different synthetic methods, which is especially true in the case of doped nanoparticles. By adjusting the temperature of thermal pyrolysis and the ratio of reagents, the maximum emission of the obtained CDot gradually shifts from blue to red light, covering the entire spectrum of light. In particular, the position of the CDot emission can be adjusted with a shift from 430 to 630 nm by controlling the degree of graphitization and the number of surface functional groups, the COOH groups. The relative quantum output of CDot luminescence with blue, green, and red radiation reach 52.6%, 35.1%, and 12.9%, respectively [9].

Significant optical properties are manifested in the strong optical absorption by carbon structure of wavelengths from the UV region with the tail extending to the visible range, up to the IR region of the spectrum, which depends on the property of the core and the excitation spectrum of polar groups, which determine the subsequent emission (luminescence) of radiation in the visible or IR regions of the spectrum [4, 6]. Thus, the fluorescence wavelength is determined by the functional property of the surface structure of the shell, the composition of polar groups, and correspondingly the manufacturing techniques, the nature of precursors [10,11].

Carbon nanoparticles, the object of study of this research, do not belong to the category of "carbon quantum dots" since they are particles of larger sizes, on the order of dozens of nm, do not belong to objects of zero dimension and possess electronic anisotropy. Moreover, spherical shape is not required for this type of carbon nanoparticles.

If the approaches to the synthesis of carbon nanoparticles are concerned [5, 12], we applied the bottom-up method with the use of molecular organic precursors, as exemplified by using citric acid (0.2 g) and urea (0.2 g) in equal proportions [12], when the required particles are obtained within one cycle. In the course of using this hydrothermal synthesis method, it became possible to control the size and properties of the resulting carbon nanoparticles [12]. The use of this approach enabled to synthesize carbon nanoparticles ranging in size from 900 nm to 70 nm, with significant absorption in the yellow-green region of the spectrum and a minimum absorption at the He-Ne laser radiation wavelength. These absorption spectra, obtained in the course of the particle experiment, determined the possibility of their use for diagnostics of speckle fields with spatially distributed singularities. Optical vortices, or singularities of the optical field, are points with zero intensity, in which when being circled around, the phase changes by 2π, 4π, etc., i.e. the phase at these points is undefined. The connection of the lines of the intensity gradient with the points of singularity, determines the formation of the grid of the intensity gradient distribution of optical field.

The magnitude of the field gradient is significantly different both for field regions of minimum intensity without singularities and for those with singularities. The differences in the values of the field gradient intensity and the optical power generated by this field form the basis of the method, which makes it possible to obtain a complete picture of the distribution of the field intensity from the diagnosed luminescence of carbon nanoparticles trapped by regions with optical singularities.

Thus, in this work, it is proposed to combine the approaches of nanochemistry and singular optics in order to obtain information about the optical field, spatial distribution of intensity and phase in real time.

3. Model Experiment and Computer Simulation Approaches

We divide the problem to be solved in this work into several stages, combining theoretical and experimental approaches. The sequence of solving is determined by the ultimate goal:

3.1. Creation of carbon nanoparticles with previously known properties detail described in our paper [12]

The synthesized nanoparticles with a size of about 60-70 nm (about $\lambda/10$) possess luminescence with an emission peak at the wavelength of 530 nm, an absorption maximum at the wavelength of 405 nm and an absorption minimum at the wavelength of 633 nm of He-Ne laser radiation. This laser is used to form a speckle pattern of the field resulting from light scattering off a surface with roughness.

3.2. Modeling a scattering surface with roughness using the correlation-singular approach [13-15]. MATHEMATICA software product was used

In our computer simulation, spline interpolation of surface elements with randomly generated heights of inhomogeneities in the interval 0 - h_{max} (h_{max} = 2 μm) was applied. In this case, the required number of pixels was selected on the selected area (50x50 μm^2), which was regulated by the scanning step. The smoothing process enabled to recreate the relief of the modeled rough surface. The simulation results were consistent with the surface profiles obtained experimentally and presented in another authors' paper [16].

To assess the simulated surface roughness [13], the location of the baseline (Fig. 1), according to existing techniques, is determined. The baseline (Fig.1, curve 1) (the line of the nominal profile) drawn along the base length (Fig.1, curve 2) and is determined as the minimization of the standard deviation of the profile points from the corresponding points of the baseline (Fig. 1).

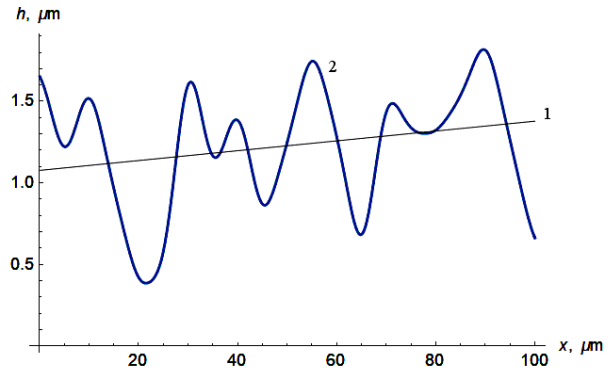

Fig. 1. Surface profile with a baseline within the same base length (object side) (color online)

The base length is determined by the contour of the surface profile, obtained at cut of the coordinate distribution of the profile inhomogeneities by the plane y = const. The baseline -1 (Fig. 1), as well as the baseline length – 2 (Fig.1), are functions of coordinates, i.e. can be written as 1 (x) and 2 (x), respectively.The coordinates of the profile z (x) are obtained as 2 (x) -1 (x) (Fig. 2)

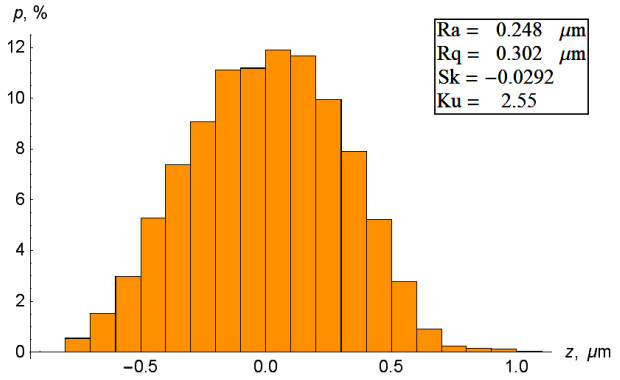

Fig. 2. Coordinates of profile points setting relative to the baseline (color online)

The resulting picture of the coordinate distribution of the surface profile points (Fig. 2) allows us to determine the profile roughness parameters:

-arithmetic mean deviation of the profile points relative to the baseline $R_a = \frac{1}{n}\sum_i |z_i|$,

--standard deviation $R_q = \sqrt{\frac{1}{n}\sum_i z_i^2}$,

-asymmetry $Sk = \frac{1}{n}\sum_i (z_i - \bar{z})^3$,

-kurtosis $Ku = \frac{1}{n}\sum_i (z_i - \bar{z})^4$ within the same baseline. The statistics of the entire surface is the following Ra = 0.248 μm, Rq = 0.302 μm, Sk = −0.0292, Ku = 2.55. The remoteness of profile points of the analyzed surface with respect to the baseline, is presented in the histogram (Fig. 3). The possibility to evaluate the corresponding profile emerges now.

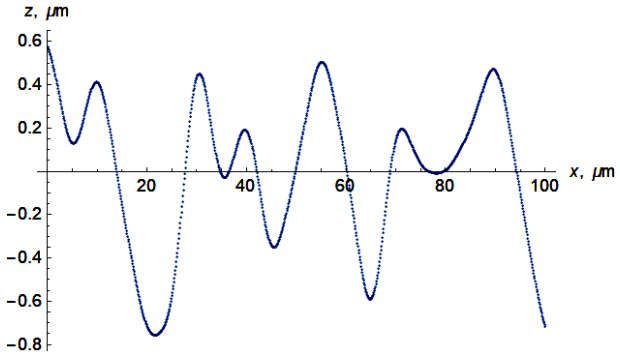

Fig. 3. The histogram describing the remoteness of the profile points (heights) relative to the baseline: z = 0 (the intersection of the baseline and the profile), the maximum number of points is determined; with distance from the baseline (z> 0, z <0) the number of profile points decreases (color online)

3.3. Obtaining and diagnosing the structure of the speckle-field from a scattering object with roughness [13]

The use of the diffraction integral in the Rayleigh-Sommerfeld approximation makes it possible to recreate the diffraction pattern. Moreover, the separation of the real $\mathrm{Re}U(\xi,\zeta)$ and the imaginary $\mathrm{Im}U(\xi,\zeta)$ parts of the calculated field allows to estimate the modulus of the field amplitude, intensity and phase, and to determine the regions of minimum intensity with singularities.

The same field assessment can be done in real time. To diagnose such distant random objects, it is proposed to use carbon nanoparticles, which, under the effect of gradient optical forces of internal energy flows, move in the optical field and are captured by the singularities of the field. A model scheme of the experiment is presented in the following figure (Fig. 4). Two laser sources with different wavelengths are used here: He-Ne laser (Fig. 4, 1) with a wavelength of 633 nm – to create a speckle field and a semiconductor laser (Figs. 4, 6) operating wavelength of which is 405 nm corresponds to maximum luminescence of carbon nanoparticles. In order to avoid the temperature effects including destroyed changes or possible particle oscillation due to their Brownian motion leading to the essential change of particle position, the temperature regime and the exposure time are controlled.

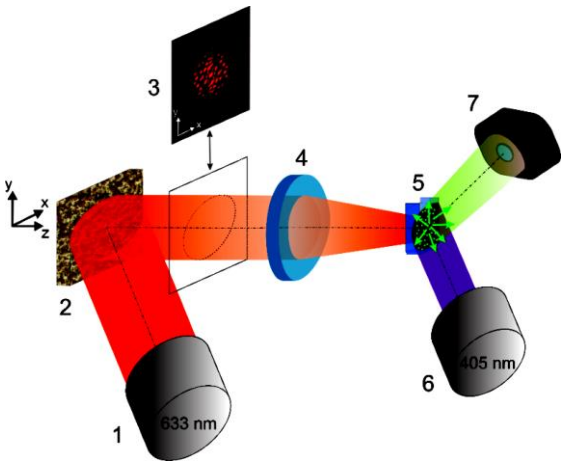

Fig. 4. Model scheme of the experiment: 1 – He-Ne laser, 2 – the studied scattering object with roughness; 3 – speckle-field, 4 – objective, 5 – cuvette with carbon nanoparticles suspended in water, 6 – semiconductor laser, 7 – CCD camera (color online)

Therefore, the laser sources used in our investigation are lasers with maximum wavelength of 405 nm and a power of 5 mW for the observation of luminescence, and a He-Ne Laser for obtaining the scattered field in which the motion of carbon particles occur. Time necessary for particle redistribution and capture is about 30 seconds, which is confirmed theoretically. The analyzed speckle field is shown in Fig. 5 (a, b) below. The field is focused in the area of the cell, with carbon nanoparticles suspended there. Focusing of laser radiation causes an increase in the longitudinal component of the field: a 3D structure is formed (Fig. 5, b). As an example, a highlighted fragment of a speckle field is shown (Fig. 5a), presented in three-dimensional space (Fig. 5, b). Under the effect of internal energy flows and the influence of gradient forces, carbon nanoparticles move along the field and are localized in the areas of minimal intensity with singularities, which is recorded by a CCD camera (Figs. 4, 7) in real time. It becomes possible to record tracks of the nanoparticles motion.

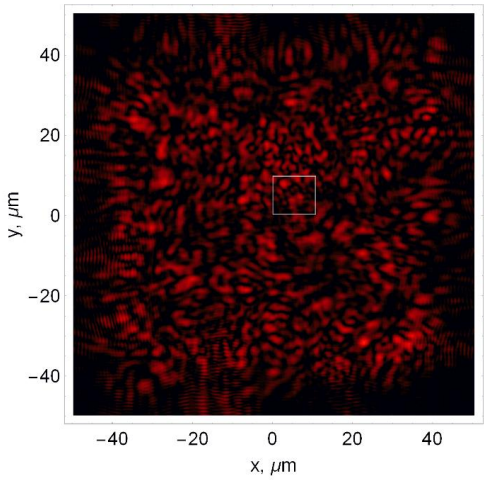

(a)

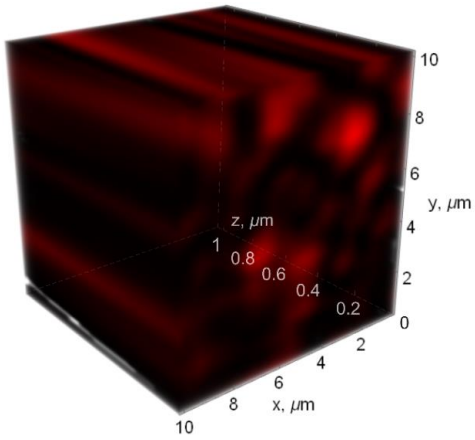

(b)

Fig. 5. Analyzed optical speckle-field: a – 2D representation, b - 3D representation. White square highlights the area of the field (a), the image of which is presented as 3D (b) (color online)

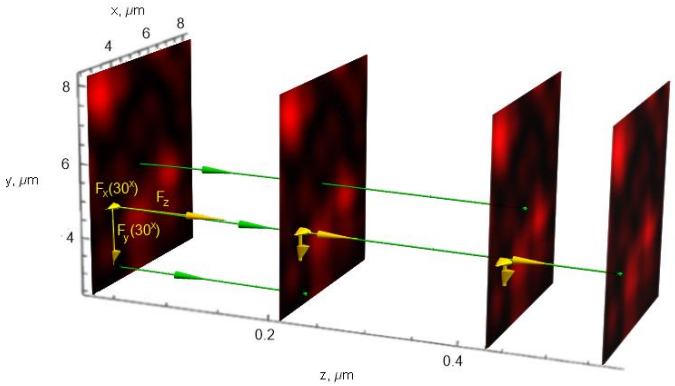

Fig. 6. Demonstration of the fragment of the field showing the tracks of carbon nanoparticles motion under the action of the components of the resulting optical power (yellow lines with arrows) before they are captured by the field singularities: F_x, F_y *– are the components of the optical power, which are formed in the transverse plane,* F_z *– in the longitudinal direction. Forces in the transverse plane are shown on a* 30^x *scale. Green lines with arrows indicate the tracks of nanoparticles motion (color online)*

As an example, the following figure (Fig. 6) shows a field element (fragment) that demonstrates the tracks of carbon nanoparticles that move under the action of optical forces until they are captured by optical vortices (singularities). Here the tracks are highlighted with green lines with arrows; yellow lines indicate the directions of action of the optical power in the longitudinal (z) - F_z and transverse ((x, y) - $F_{x,y}$ directions (the algorithm for calculating the optical force components is given below). In order to visualize the forces in the figure, the sizes of the vectors indicating the directions of the acting forces in the transverse plane were increased by 30^x.

The length of the track will naturally be different depending on the initial localization of nanoparticles and the distance from the point of capture.

The concentration of particles and the luminescence intensity also differ substantially in the regions with and without singularities.

3.4. Restoration of the distribution of the intensity of the optical field

The next stage of our paper was to restore the intensity of the field of optical radiation scattered by the object under study by means of analyzing the track of luminescent nanoparticles, their length and direction. The direct motion of particles was determined by the force (Fig. 6) depending on the ratio of components of the resulting optical force in the transverse plane and in the longitudinal direction [17,18] (F_{x,y,z_i}), which, in its turn, is determined by the contribution of gradient, scattering and absorbing components of optical force and force of friction ($6\pi r\eta v_{x,y,z_i}$) of a moving nanoparticle suspended in water. Here *i* is a separately isolated nanoparticle.

The direction of each of the components of the force differs significantly. If we consider the transverse plane (XY), then the gradient force (the gradient component of the resulting optical force) $\vec{F}_{grad} = -\frac{\alpha'}{2} n \nabla \frac{|E|^2}{2}$ will be determinative. In the longitudinal direction OZ, the motion of a carbon nanoparticle is set, as a rule, by the absorbing (absorbing component of the resulting optical force) $\vec{F}_{abs} = k\alpha'' \frac{n\langle \vec{S} \rangle}{c}$ and scattering (scattering component of the resulting optical force) $\vec{F}_{scatt} = \frac{k^4 |\alpha|^2}{4\pi} \frac{n\langle \vec{S} \rangle}{c}$ forces, i.e., by the directions of the action of Poynting vector. Here $k = \frac{2\pi}{\lambda}$ - wavenumber, particle polarizability $\alpha = \alpha' + i\alpha''$, which depends on the optical parameters of the synthesized nanoparticles: refractive index (n) and absorption coefficient (κ).

The action direction of the resulting optical force ($\vec{F} = \vec{F}_{grad} + \vec{F}_{scatt} + \vec{F}_{abs}$) changes depending on the gradients of internal energy flows and on the direction of the Poynting vector action.

Taking into account the Cartesian components, the equation of motion for the *i-th* particle has the form $m\frac{dv_{x,y,z_i}}{dt} = F_{x,y,z_i} - 6\pi r\eta v_{x,y,z_i}$. The distribution of the optical force components for individual carbon nanoparticles is shown in Fig. 6.

The change of the coordinate of a particle within time is written as $x, y, z_i(t) = x, y, z_i(t_0) + v_{x,y,z_i} t + \frac{dv_{x,y,z_i}}{dt} \cdot \frac{t^2}{2}$. The joint solution of the system of the above equations makes it possible to reconstruct the coordinate (pixel-by-pixel) intensity distribution, following the pixel-by-pixel analysis of the localization of nanoparticles, registered by the CCD-camera. The initial moment of observation is taken as the zero value. The result essentially depends on the amount (concentration) of nanoparticles that take part in the simulation. In the experiment, the concentration of nanoparticles in a water solution was controlled by its optical density. Next figure (Fig. 7) represents the reproduction accuracy for different intensity values which changes within the interval of 90% - 97%. These results demonstrate a rather high accuracy of the proposed algorithm of intensity reproduction.

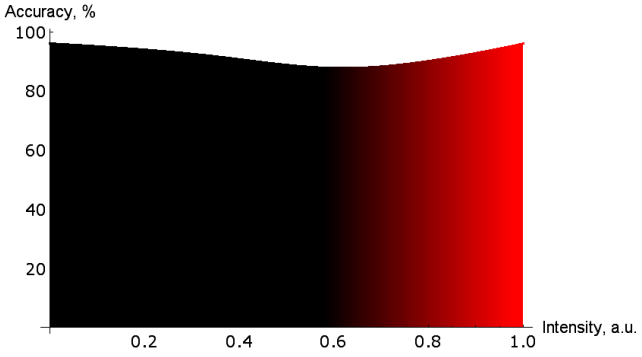

Fig.7. Accuracy of intensity reproduction for different values of intensity: (intensity axis: "0" corresponds to minimum intensity, "1" to maximum value; accuracy axis describes the diapason of accuracy variation (color online)

3.5. Obtaining a phase map of the optical field

The use of the Hilbert transform [19] makes it possible to recover information about the phase distribution of the optical field under study, taking into account the localization of singularity points. Unfortunately, imposing the Hilbert filters on the intensity distribution of the optical field partially smoothens the phase information particularly at the points where the phase is undefined, i.e., at the points of singularity [19].

Therefore, the latter, as follows from the above-proposed approach, these points are found experimentally from the luminescence of the trapped carbon nanoparticles and thus supplement the lost information about the phase.

During the simulation the kernel of the two-dimensional discrete Hilbert transform was used, which was traditionally represented in the cotangent form [20-22]

$$SI = \frac{2}{N_1 N_2} \sum_{k_1=1,3...}^{N_1-1} \sum_{k_2=1,3...}^{N_2-1} SR(k_1 k_2) \left[\cot \frac{\pi(i_1 - k_1)}{N_1} + \cot \frac{\pi(i_2 - k_2)}{N_2} \right],$$

where i_1, i_2 – take even values;

$$SI = \frac{2}{N_1 N_2} \sum_{k_1=1,3...}^{N_1-1} \sum_{k_2=0,2...}^{N_2-1} SR(k_1 k_2) \left[\cot \frac{\pi(i_1 - k_1)}{N_1} + \cot \frac{\pi(i_2 - k_2)}{N_2} \right],$$

where i_1 takes even values, while i_2 – odd ones;

$$SI = \frac{2}{N_1 N_2} \sum_{k_1=0,2...}^{N_1-1} \sum_{k_2=1,3...}^{N_2-1} SR(k_1 k_2) \left[\cot \frac{\pi(i_1 - k_1)}{N_1} + \cot \frac{\pi(i_2 - k_2)}{N_2} \right],$$

, here i_1 takes odd values, and i_2 – even ones;

$$SI = \frac{2}{N_1 N_2} \sum_{k_1=0,2...}^{N_1-1} \sum_{k_2=0,2...}^{N_2-1} SR(k_1 k_2) \left[\cot \frac{\pi(i_1 - k_1)}{N_1} + \cot \frac{\pi(i_2 - k_2)}{N_2} \right],$$

, here i_1, i_2 take odd values.

Convolution of the transform kernel with the analyzed image allows to obtain the phase map (Fig. 8, a) with a certain accuracy (Fig. 8, b). As can be seen from this figure (Fig. 8, b), the phase with values of 0, 2π, that corresponds to the regions of the intensity minimum, where the singularity points are localized, is restored with a lower accuracy of about of 50-60%, in contrast to other phase regions, for which the phase restoration accuracy reaches 80-90%. Therefore, determining the location of carbon nanoparticles significantly improves the overall picture of the phase recovery of the studied object.

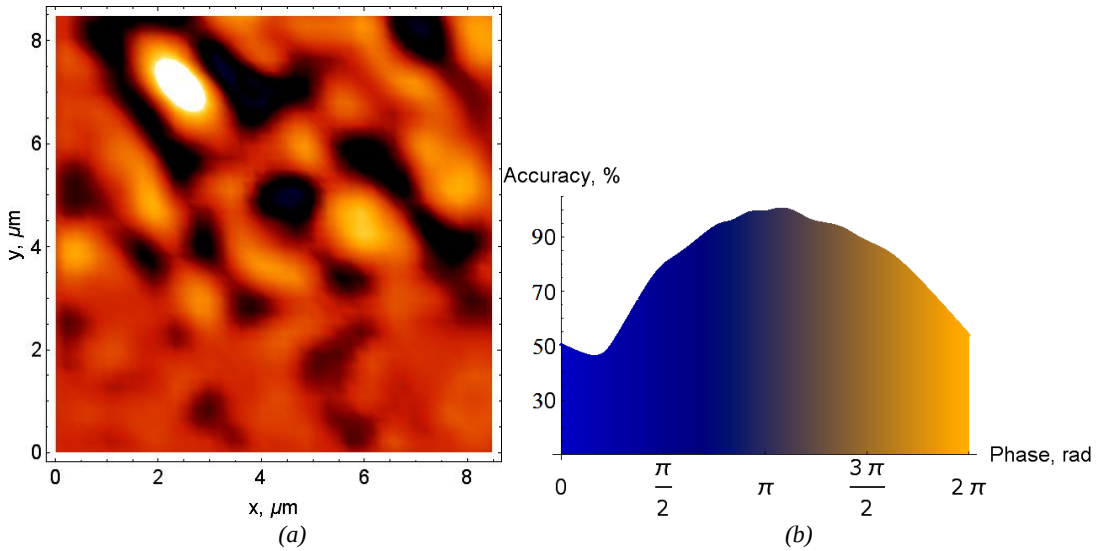

Fig. 8. Reconstructed phase map obtained by Hilbert transform (a), with accuracy of reconstruction (b) (color online)

4. Conclusions

The results proposed in this research open up new possibilities for the analysis, study and diagnostics of complex optical speckle fields obtained from distant scattering objects in real time. Carbon nanoparticles about $\lambda/10$ in size were used as markers of optical field singularities. The proposed model of the model experiment enabled to record the tracks of nanoparticles motion until the moment of their capturing by the field singularities, which was visualized by the bright luminescence of these particles. Internal energy flows, distributed in the field, set the optical force, ensuring the motion of the particles in the field. It was suggested to use the information on the pixel-by-pixel distribution of the tracks of moving particles and the location of singularity points to reconstruct the intensity of the optical field. The phase of the studied field was reconstructed by the Hilbert transform when location of phase singularities was pointed by carbon nanoparticles.

References

[1] A. A. Kokorina, E. S. Prikhozhdenko, G. B. Sukhorukov, A. V. Sapelkin, I. Yu. Goryacheva, Russ. Chem. Rev. **86**(11), 1157 (2017).

[2] C. J. Reckmeier, J. Schneider, A. S. Susha, A. L. Rogach, Optics Express **24**(2), A312 (2016).

[3] O. M. Marago, P. G. Gucciardi, Fr. Bonaccorso, M. A. Iatì, Physica E. Low-dimensional Systems and Nanostructures **40**(7), 2347 (2007).

[4] Yu. Choi, Ye. Choi, Oh-H. Kwon, B.-S. Kim, Chemistry - An Asian Journal **13**(6), 586 (2018).

[5] I. Y. Goryacheva, A. V. Sapelkin, G. B. Sukhorukov, Trends in Analytical Chemistry **90**, 27 (2017).

[6] X. Miao, D. Qu, D. Yang, B. Nie, Y. Zhao, H. Fan, Z. Sun, Adv. Mater. **30**(1), 1704740 (2018).

[7] A. Cayuela, M. L. Soriano, C. Carrillo-Carrion, M. Valcarcel, Chemical Communications **52**(7), 1311 (2016).

[8] Y. Wang, A. Hu, Journal of Materials Chemistry C **2**(34), 6921 (2014).

[9] O. V. Angelsky, C. Yu. Zenkova, D. I. Ivanskyi, V. M. Tkachuk, Proc. SPIE **11509**, 115090N (2020).
[10] K. P. Suman, Carbon **88**, 86 (2015).
[11] L. Ge, N. Pan, J. Jin, P. Wang, G. E. LeCroy, W. Liang, L. Yang, L. R. Teisl, Y. Tang, Y.-P. Sun, J. Phys. Chem. C **122**(37), 21667 (2018).
[12] P. P. Maksimyak, C. Yu. Zenkova, V. M. Tkachuk, Physics and chemistry of solid state **21**(1), 13 (2020).
[13] O. V. Angelsky, P. P. Maksimyak, S. Hanson, The Use of Optical-Correlation Techniques for Characterizing Scattering Object and Media. Bellingham: SPIE Press PM71, 194 (1999).
[14] O. V. Angelsky, P. P. Maksimyak, Applied Optics **31**(1), 140 (1992).
[15] O. V. Angelsky, P. P.Maksimyak, Applied Optics **31**(22), 4417 (1992).
[16] O. V. Angelsky, P. P. Maksimyak, V. V. Ryukhtin, S. G. Hanson, Applied Optics **40**(31), 5693 (2001).
[17] C. Zenkova, I. Soltys, P. Angelsky, Optica Applicata **2**(43), 297 (2013).
[18] C. Yu. Zenkova, M. P. Gorsky, I. V. Soltys, P. O. Angelsky, Applied Optics **51**(10), C38 (2012).
[19] H. P. Baltes, Inverse Source Problems in Optics, Publisher Springer-Verlag Berlin Heidelberg, 204 (1978).
[20] C. Yu. Zenkova, M. P. Gorsky, P. A. Ryabiy, Optica Applicata **46**(1), 153(2016).
[21] C. Yu. Zenkova, M. P. Gorsky, P. A. Ryabiy, Romanian Reports in Physics **67**(4), 1401 (2015).
[22] C. Yu. Zenkova, M. P. Gorsky, P. A. Ryabiy, A. O. Angelskaya, Appl. Opt. **55**(12), B78 (2016).

*Corresponding author: k.zenkova@chnu.edu.ua